HYDROPHOBIC FERROCENE DERIVATIVES AS POTENTIAL STANDARDS IN ELECTROCHEMISTRY

Jaroslav PODLAHA[a1], Petr STEPNICKA[a2], Robert GYEPES[a3], Vladimir MARECEK[b1], Alexander LHOTSKY[b2], Miroslav POLASEK[b3], Jiri KUBISTA[b] and Martin NEJEZCHLEBA[c]

[a] *Department of Inorganic Chemistry, Charles University, 128 40 Prague 2, Czech Republic; e-mail:* [1] *podlaha@prfdec.natur.cuni.cz,* [2] *stepnic@prfdec.natur.cuni.cz,* [3] *gyepes@prfdec.natur.cuni.cz*

[b] *J. Heyrovsky Institute of Physical Chemistry, Academy of Sciences of the Czech Republic, 182 28 Prague 8, Czech Republic; e-mail:* [1] *marecek@jh-inst.cas.cz,* [2] *sum@jh-inst.cas.cz,* [3] *hanus@jh-inst.cas.cz*

[c] *Joint Laboratory of Mössbauer Spectroscopy, Charles University, V Hole¿oviçkách 2, 182 00 Prague 8, Czech Republic; e-mail: nejezchl@hp03.troja.mff.cuni.cz*

Received October 3, 1996
Accepted October 23, 1996

Dedicated to Dr Karel Mach on the occasion of his 60th birthday.

Ferrocene (FcH) derivatives monosubstituted by palmitoyl (**1**), hexadecyl (**2**), 1-adamantoyl (**3**) or 1-adamantylmethyl (**4**) groups were sythesized and characterized by NMR, mass and ^{57}Fe Mössbauer spectroscopy. The structure of 1-adamantoylferrocene was determined by single-crystal X-ray diffraction. Cyclic voltammetry on gold and glass-like carbon electrodes demonstrated that the compounds can serve as electrochemical standards for special cases since their ferrocene/ferricinium redox potential remains stable and reversible, while the properties such as solubility, diffusion coefficients and surface tension are strongly solvent-dependent.

Key words: Substituted ferrocenes; Electrochemistry; Crystal structure; Mössbauer spectroscopy; Mass spectroscopy.

Due to the reversibility and stability of the redox potential and the solubility in many polar solvents, the ferrocene/ferricinium couple became the indispensable potential standard in electrochemistry (see, e.g., ref.[1]). Its use in ferrocene-containing polymer-coated electrodes is also well documented[2]. Nevertheless, special needs may arise in the cases of, e.g., unusual solubility, surface tension and other requirements. These properties of the ferrocene/ferricinium redox pair can be most easily modified by the introduction of proper substituents at the cyclopentadienyl ring(s)[3,4]. In this paper, we describe the synthesis, characterization and basic electrochemical characterization of ferrocenes bearing hydrophobic substituents. These include a long aliphatic chain or the 1-adamantylmethyl group bringing, respectively, large and small surface activity. Some

of these derivatives and their synthetic precursors are already known but have been insufficiently characterized; their electrochemical behavior is unknown.

EXPERIMENTAL

Synthetic work was carried out by standard inert-atmosphere procedures using purified and dried solvents. Melting points are uncorrected. ^{1}H NMR (200.06 MHz) spectra were recorded on a Varian Unity 200 instrument in $CDCl_3$ solution at ambient temperature with TMS as internal standard; IR spectra in Nujol mulls were measured in the range of 400–4 000 cm^{-1} on an FT IR ATI Mattson Genesis instrument.

Low resolution mass spectra were recorded on VG-7070E double focusing mass spectrometer (EB geometry, electron ionization mode, electron energy 70 eV, ionizing current 100 μA, source temperature 200 °C, accelerating voltage 6 kV). Metastable ion decompositions in the first field-free region were observed using linked scanning of electrostatic and magnetic analyzers at constant B/E (daughter ion scan), at constant B^2/E (parent ion scan) and at constant $B/[E(1 - E/E_0)^{-1/2}]$ (constant neutral loss scan). Accurate mass determinations were performed on Jeol JMS-D100 double focusing mass spectrometer (electron energy 80 eV, ionizing current 300 μA, source temperature 200 °C, accelerating voltage 3 kV) using peak matching method with perfluorokerosene as internal standard. The instrument was tuned to resolution of 10 000 (50% valley).

^{57}Fe transmission Mössbauer spectra were recorded in constant acceleration mode, using the ^{57}Co isotope deposited in a Cr matrix as the source of radiation. All measurements were carried out at room temperature (500 channels for the range ⟨–4.8;+4.8⟩ mm s^{-1}). α-Fe was used for the velocity scale calibration and as the reference for the isomer shift values. The Mössbauer parameters were evaluated by a curve fitting procedure (Lorentzian lineshape).

Electrochemical measurements were carried out at room temperature in argon atmosphere with $1 . 10^{-3}$ mol dm^{-3} nitrobenzene solutions containing $1 . 10^{-2}$ mol dm^{-3} Bu_4NPF_6 as the supporting electrolyte. Ferrocene and its derivatives **1–4** were studied by voltammetry on rotating disk gold (Au; geometric area of 3.25 mm^2, 23 s^{-1}) and glass-like carbon electrodes (GC; 7.95 mm^2, 23 s^{-1}) and by cyclic voltammetry (CV) on stationary Au and GC electrodes at polarization rates in the range of 10–200 mV s^{-1}. The three-electrode system used consisted of WINTER diaplast 1-SS (Hamburg, Germany) working electrode, platinum sheet counter electrode and Ag/AgCl reference electrode (immersed in 10^{-2} mol dm^{-3} aqueous Bu_4NCl solution, which was in contact with ferrocene-containing organic phase). AC voltammetry measurements were performed on a Solartron 1250 Frequency Response Analyzer and 1286 Electrochemical Interface (Solartron Schlumberger, U.K.) with polarization rates of 2.5 mV s^{-1}. AC voltammetry curves were registered on a personal computer via RS232 serial port. Diffusion coefficients were calculated from CV data using the procedure given in ref.[5].

Palmitoylferrocene[6] (**1**)

The mixture of palmitic acid (6.4 g, 25 mmol), thionyl chloride (5.6 g, 78 mmol) and five drops of dimethylformamide was left to stand for 20 h at room temperature. Excess of $SOCl_2$ was distilled off at ambient and then at reduced pressure. The residue of crude palmitoyl chloride together with $AlCl_3$ (2.7 g, 20 mmol) was added to the solution of ferrocene (3.7 g, 20 mmol) in dichloromethane (50 ml). After stirring overnight, water (20 ml) was added, the organic layer was separated and the aqueous layer was extracted with dichloromethane (2 × 30 ml). The combined organic layers were washed by aqueous $NaHCO_3$ followed by water and dried over $MgSO_4$. Evaporation in vacuo and then repeated evaporation with benzene, dissolution of the solidified residue in hot methanol (100 ml), filtration (charcoal) and crystallization in ice-box gave crude palmitoylferrocene. This was

purified by crystallization first from hot methanol containing 1% KOH and then from pure methanol to give 2.1 g (25%) of orange solid, m.p. 57.5–58.5 °C (ref.[6] gives 59.0–59.8 °C). For $C_{26}H_{40}FeO$ (424.5) calculated: 73.57% C, 9.40% H; found: 73.42% C, 9.52% H. ^{1}H NMR spectrum: 0.88 bt, 3 H, J = 6.6 ($COCH_2CH_2(CH_2)_{12}C\mathbf{H}_3$); 1.18–1.44 bm, 24 H ($COCH_2CH_2(C\mathbf{H}_2)_{12}CH_3$); 1.70 qi, 2 H, J = 7.3 ($COCH_2C\mathbf{H}_2(CH_2)_{12}CH_3$); 2.69 t, 2 H, J = 7.3 ($COC\mathbf{H}_2CH_2(CH_2)_{12}CH_3$); 4.19 s, 5 H ($C_5H_5$); 4.49 m, 2 H ($C_5H_4$); 4.78 m, 2 H ($C_5H_4$). IR spectrum: 3 102 w, 1 670 s, 1 306 w, 1 286 w, 1 268 m, 1 248 m, 1 230 m, 1 107 m, 1 075 m, 2 1023 m, 1 001 m, 819 m, 533 m, 498 m, 479 m. Mass spectrum, *m/z* (abund.%): 424 ($M^{+\bullet}$; 100), 406 (2), 228 (9), 213 (6), 199 (2), 186 (15), 185 (10), 129 (8), 121 (10), 69 (3), 56 (3), 55 (5), 43 (7); HRMS, measured (calculated) *m/z*: 424.2444 (424.2428, $C_{26}H_{40}OFe$); 406.2323 (406.2323, $C_{26}H_{38}Fe$); 228.0236 (228.0237, $C_{12}H_{12}OFe$); 212.9993 (213.0003, $C_{11}H_9OFe$); 199.0209 (199.0210, ($C_{11}H_{11}Fe$); 186.0124 (186.0132, $C_{10}H_{10}Fe$); 185.0054 (185.0054, $C_{10}H_9Fe$); 129.0702 (129.0704, $C_{10}H_9$); 120.9746 (120.9741, C_5H_5Fe).

Hexadecylferrocene (**2**)

Following the general method for reduction of ketones[6], the mixture of $LiAlH_4$ (0.19 g, 5.0 mmol), $AlCl_3$ (0.54 g, 4.0 mmol) and diethyl ether (15 ml) was stirred for 5 min and then palmitoylferrocene (0.637 g, 1.50 mmol) in Et_2O (10 ml) was added in one portion. After stirring for 20 min at room temperature, water (5 ml) and then 6 M HCl (5 ml) was added. After dilution with Et_2O (20 ml), the organic layer was washed with water, dried over $MgSO_4$ and evaporated in vacuo. Purification by chromatography (Al_2O_3, Et_2O) provided, after evaporation, 0.541 g (88%) of the pure product as yellow solid, m.p. 43–45 °C (ref.[6] gives 55.0–55.6 °C). For $C_{26}H_{42}Fe$ (410.5) calculated: 76.08% C, 10.31% H; found: 75.79% C, 10.33% H. ^{1}H NMR spectrum: 0.88 bt, 3 H, J = 6.6 ($C_5H_4CH_2(CH_2)_{14}C\mathbf{H}_3$); 1.10–1.55 m, 28 H ($C_5H_4CH_2(C\mathbf{H}_2)_{14}CH_3$); 2.30 bt, 2 H, J = 7.6 ($C_5H_4C\mathbf{H}_2(CH_2)_{14}CH_3$); 4.05 m, 4 H ($C_5H_4$); 4.10 s, 5 H ($C_5H_5$). IR spectrum: 3 094 w, 3 079 w, 1 105 s, 1 047 m, 1 027 m, 1 000 m, 919 m, 819 s, 814 s, 715 m, 520 m, 507 m, 484 m. Mass spectrum, *m/z* (abund.%): 410 ($M^{+\bullet}$; 100), 212 (2), 199 (14), 186 (4), 134 (2), 121 (8), 69 (2), 56 (2), 43 (4); HRMS, measured (calculated) *m/z*: 410.2642 (410.2634, $C_{26}H_{42}Fe$); 212.0288 (212.0284, $C_{12}H_{12}Fe$); 199.0209 (199.0210, $C_{11}H_{11}Fe$); 186.0131 (186.0132, $C_{10}H_{10}Fe$); 120.9746 (120.9741, C_5H_5Fe).

(1-Adamantoyl)ferrocene[2] (**3**)

The mixture of 1-adamantanecarboxylic acid (1.82 g, 10.1 mmol), thionyl chloride (11 ml, ~150 mmol) and 1 drop of dimethylformamide was refluxed for 4 h. Excess $SOCl_2$ was distilled off (oil bath) to leave crude 1-adamantoyl chloride. Heptane (30 ml), ferrocene (1.88 g, 10.1 mmol) and $Mo(CO)_5$ (0.264 g, 1.00 mmol) was added, the resulting mixture was refluxed for 40 h and filtered while hot. The solid residue was washed with hot heptane (3 × 10 ml), the combined filtrates were evaporated in vacuo to dryness and the residue dissolved in chloroform (50 ml). After washing with aqueous 2 M NaOH and water, drying over $MgSO_4$ and evaporation in vacuo, the crude product was dissolved in toluene and chromatographed on silica gel (toluene–petroleum ether 1 : 1 eluted mainly unreacted ferrocene; then toluene–diethyl ether 1 : 1 eluted the product). A black impurity remained on the top of the column; no diacyl derivative was present. The first fraction gave, after repeated chromatography, a further crop of the product (total amount of regenerated ferrocene was 0.68 g). The yield of rusty-red (1-adamantoyl)ferrocene was 71% (calculated for the reacted ferrocene). Analytical sample was prepared by vacuum sublimation. For $C_{21}H_{24}FeO$ (348.3) calculated: 72.42% C, 6.95% H; found: 72.40% C, 6.97% H. ^{1}H NMR spectrum: 1.55–2.16 m, 15 H (adamantyl); 4.18 s, 5 H (C_5H_5); 4.46 m, 2 H (C_5H_4); 4.90 m, 2 H (C_5H_4). IR spectrum: 3 115 w, 1 641 s, 1 275 s, 1 250 s, 1 184 m, 1 107 m, 1 051 m, 1 030 m, 822 m, 793 m, 764 m, 506 m, 499 m, 488 m, 470 w. Mass spectrum, *m/z* (abund.%): 348 ($M^{+\bullet}$; 100), 320 (2), 213 (32), 186 (6), 185 (22), 135 (10), 129 (17), 121 (9), 93 (6),

79 (7), 67 (4), 56 (7), 41 (4); HRMS, measured (calculated) *m/z*: 348.1178 (348.1176, $C_{21}H_{24}FeO$); 320.1237 (320.1227, $C_{20}H_{24}Fe$); 12.9999 (213.0003, $C_{11}H_9FeO$); 185.0054 (185.0054, $C_{10}H_9Fe$); 135.1170 (135.1174, $C_{10}H_{15}$); 129.0702 (129.0704, $C_{10}H_9$); 120.9742 (120.9741, C_5H_5Fe).

(1-Adamantylmethyl)ferrocene (**4**)

Similarly as above, the mixture of $LiAlH_4$ (0.24 g, 6.3 mmol), $AlCl_3$ (0.81 g, 6.1 mmol) and diethyl ether (10 ml) was stirred for 5 min and then the suspension of (1-adamantoyl)ferrocene (1.041 g, 2.99 mmol) in Et_2O (25 ml) was added during 5 min. After stirring for 30 min at room temperature, further $LiAlH_4$ (100 mg) was added and stirring continued for 15 min. The reaction was quenched by addition of water (5 ml) and 6 M HCl (5 ml). Then Et_2O (30 ml) was added and the aqueous layer was extracted with Et_2O, the combined organic layer was washed with water, dried over $MgSO_4$ and evaporated. Chromatography on a short column of Al_2O_3 (elution with Et_2O) and evaporation provided 0.946 g (95%) of the product as a yellow-orange waxy solid. Analytical sample was purified by vacuum sublimation. For $C_{21}H_{26}Fe$ (334.3) calculated: 75.45% C, 7.84% H; found: 75.27% C, 8.08% H. ^{1}H NMR spectrum: 1.25–1.95 m, 15 H (adamantyl); 2.13 s, 2 H (CH_2); 4.00 bs, 4.03 bs and 4.08 s, 9 H (C_5H_4 and C_5H_5). IR spectrum: 3 090 m, 1 344 m, 1 314 m, 1 260 m, 1 105 s, 1 039 m, 1 022 m, 1 000 m, 805 s, 500 s, 485 s, 452 m, 444 w. Mass spectrum, *m/z* (abund.%): 334 ($M^{\bullet+}$; 100), 199 (39), 186 (4), 135 (7), 134 (3), 121 (22), 93 (5), 79 (6), 67 (3), 56 (7), 41 (3); HRMS, measured (calculated) *m/z*: 334.1382 (334.1390, $C_{21}H_{26}Fe$); 199.0209 (199.0210, $C_{11}H_{11}Fe$); 186.0124 (186.0132, $C_{10}H_{10}Fe$); 135.1170 (135.1174, $C_{10}H_{15}$); 120.9742 (120.9741, C_5H_5Fe).

X-Ray Crystallography

Needle-shaped, extremely fragile crystals of **3** were grown from toluene by slow evaporation at room temperature. They were isolated by careful washing with petroleum ether, decantation and drying on air. The diffractions were measured on a CAD4-MACHIII four circle diffractometer at 293(2) K using graphite-monochromatized MoKα radiation (λ = 0.71069 Å) and θ–2θ scan. The structure was solved by direct methods (SIR92, ref.[7]) yielding the positions of all non-hydrogen atoms. Hydrogen atoms were identified on the difference electron density map and isotropically refined. The refinement (SHELXL93, ref.[8]) by minimization of the function $\Sigma w(|F_o| - |F_c|)^2$, where $w = [\sigma^2(F_o^2) + (0.0408P)^2]^{-1}$ and $P = (F_o^2 + 2F_c^2)/3$, converged to the values summarized in Table I. The coordinates and the mean thermal factors of non-hydrogen atoms are given in Table II, the selected interatomic distances and angles in Table III. Tables of the observed and calculated structure factors, anisotropic thermal factors of non-hydrogen atoms and coordinates of hydrogen atoms with their isotropic thermal factors in the standard form of the CIF files produced by SHELXL93 can be obtained from the authors upon request.

RESULTS AND DISCUSSION

The synthetic work (see Scheme 1) presented above is either the optimization of the already known but only incompletely documented procedures, or the application of a general method to the new compounds. The compounds were characterized by a number of methods. Their IR and NMR spectra are in accord with the proposed structures.

All compounds studied exhibit a strong molecular ion in their conventional electron ionization mass spectra. Another common feature observed for **1–4** is the loss of the R substituent from their molecular ions, producing ions at *m/z* 213 (**1** and **3**) and 199

(**2** and **4**), respectively. The fragment ions at *m/z* 213, originating from $\mathbf{1}^{\ddagger}$ and $\mathbf{3}^{\ddagger}$, then eliminate one molecule of carbon monoxide. The resulting ions at *m/z* 185 decompose either by the loss of Fe atom or of the C_5H_4 fragment (Scheme 2). The ions at *m/z* 199 resulting from $\mathbf{2}^{\ddagger}$ and $\mathbf{4}^{\ddagger}$ eliminate C_6H_6 (probably benzene as the product of ring expansion) or C_5H_5. The presence of ferrocene molecular ions at *m/z* 186 in the spectra of **2** and **4** is also characteristic (Scheme 3). One of the most intense fragment ions in the mass spectrum of **1** (*m/z* 228) is a product of McLafferty rearrangement (Scheme 4). This rearrangement is impossible for **3** since three β-bonds have to be cleaved. The decomposition pathways of ions at *m/z* 228, via ions at *m/z* 213, 185 etc., are very similar to the fragmentation of acetylferrocene[9] (Scheme 2 and 4). This fact supports the assignment of the structure of ions at *m/z* 228 as shown in Scheme 4. The charac-

TABLE I
Crystallographic data, measurement and structure refinement for **3**[a]

Crystal system, space group	orthorhombic, $P2_12_12_1$ (No.19)
a, *b*, *c*, Å	10.672(1), 12.074(1), 12.775(4)
V, Å^3; *Z*	1 646.1(5); 4
ρ_{calc}, g cm^{-3}	1.405
Absorption coefficient μ, mm^{-1}	0.92
Diffractions for lattice parameters determination	25; $24 \le 2\theta \le 26°$
Crystal dimensions, mm	$0.05 \times 0.13 \times 0.50$
Diffractions collected; 2θ range	1 686; 4.6 – 49.8°
h, *k*, *l* range	0→12, 0→14, 0→15
Unique diffractions	1 665
Diffractions observed along $\lvert F_o\rvert > 4\sigma(F_o)$ criterion	1 313
Standard diffractions	3 monitored every 1 h; intensity fluctuation ±2%
F(000)	736
No. of refined parameters	301
Max(Δ/σ) for the last LS cycle	0.00
R(*F*), *wR*(F^2), %; *S* for all diffractions	6.34, 7.50; 1.06
R(*F*), *wR*(F^2), %; *S* for observed diffractions	3.00, 6.67; 1.09
R(σ), %	4.52
Max. and min. heights in final Δρ map, e Å^{-3}	0.66; –0.22
Flack's enantiomorph parameter	0.02(3)

[a] $R(F) = \Sigma \lvert\lvert F_o\rvert - \lvert F_c\rvert\rvert / \Sigma \lvert F_o\rvert$, $wR(F^2) = [\Sigma(w(F_o^2 - F_c^2)^2)/(\Sigma w(F_o^2)^2]^{1/2}$, $S = [\Sigma(w(F_o^2 - F_c^2)^2)/(N_{diffrs} - N_{params})]^{1/2}$.

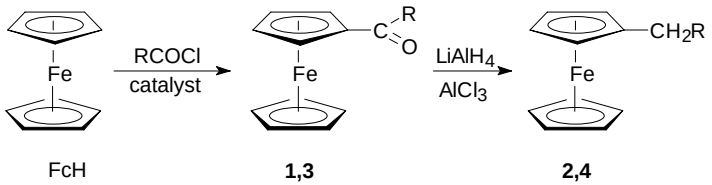

	R	catalyst
1,2	$(CH_2)_{14}CH_3$	$AlCl_3$
3,4	1-adamantyl	$Mo(CO)_5$

SCHEME 1

teristic feature of the mass spectra of 1-adamantyl-containing compounds **3** and **4** is the presence of abundant ions at *m/z* 135 due to the high stability of the adamantyl cation. On the contrary, the long aliphatic-chain derivatives **1** and **2** display a homologous series of low abundant ions $(M - C_nH_{2n+2})^{+\bullet}$ in their mass spectra. Such relatively unusual loss of alkane molecules is probably made possible by a hydrogen transfer, mediated through the iron atom.

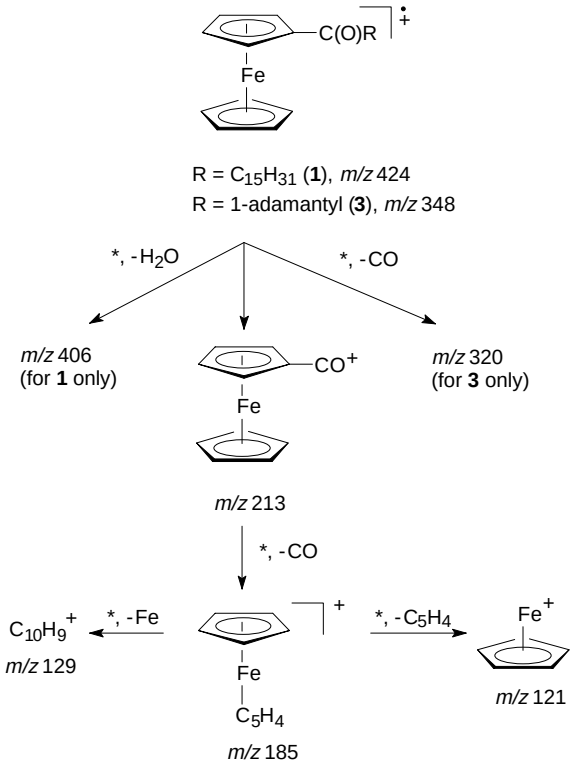

SCHEME 2

The molecular structure of **3** (as the only derivative for which single crystals of sufficient quality could be obtained) is depicted on Fig. 1. In the crystal, the molecules are packed at normal van der Waals distances and, hence, the distortion from the ideal geometry is intramolecular in nature. The central C(1)–C(11)(=O)–C(12) unit is planar within ±0.016(4) Å with normal bond distances of a ketone, albeit with a little exotic substituents. The carbon–carbon bond lengths within this unit are, however, significantly unequal, the bond to the ferrocenyl substituent being shorter by 7 estimated

TABLE II
Atomic coordinates (. 10^4) and equivalent isotropic displacement parameters (. 10^3 Å^2) for **3**. U_{eq} is defined as one third of the trace of the orthogonalized $\boldsymbol{U}_{ij}$ tensor

Atom	*x*	*y*	*z*	U_{eq}
Fe	4755(1)	–1270(1)	6173(1)	35(1)
O	2361(4)	–590(3)	8129(2)	63(1)
C1	2907(4)	–1338(4)	6511(3)	33(1)
C2	3108(4)	–1373(4)	5386(3)	36(1)
C3	3846(5)	–2306(4)	5184(4)	44(1)
C4	4099(5)	–2857(4)	6121(4)	47(1)
C5	3535(5)	–2264(4)	6944(4)	41(1)
C6	5452(6)	188(6)	6714(6)	71(2)
C7	5655(7)	103(6)	5638(6)	76(2)
C8	6378(6)	–843(6)	5464(6)	68(2)
C9	6641(5)	–1338(7)	6420(5)	65(2)
C10	6054(6)	–691(7)	7198(5)	68(2)
C11	2245(4)	–517(4)	7182(3)	38(1)
C12	1372(4)	360(4)	6718(3)	33(1)
C13	373(5)	–158(4)	6014(4)	40(1)
C14	–492(5)	737(5)	5585(4)	52(2)
C15	–1154(4)	1330(5)	6483(4)	45(1)
C16	–187(5)	1857(4)	7189(4)	45(1)
C17	580(5)	2703(4)	6567(5)	50(1)
C18	1238(5)	2129(4)	5663(4)	51(1)
C19	2127(4)	1223(4)	6092(4)	39(1)
C20	693(5)	973(4)	7617(4)	43(1)
C21	280(6)	1577(5)	4949(4)	54(1)

standard deviations than that to the adamantyl. The ferrocenyl substituent is characterized by nearly parallel, planar cyclopentadienyl rings (the dihedral angle of the mean cyclopentadienyl planes is 1.8(3)°), which are mutually oriented in an almost perfectly eclipsed conformation. In ferrocene and its derivatives which are free of other sterical constraints, the energy of the isolated molecule is known to be almost invariant towards the rotation of cyclopentadienyl rings along the D_5 axis. Hence, the particular arrangement (eclipsed vs staggered) is dictated by more subtle effects, the inter- and intramolecular van der Waals forces being prominent. In the present structure, there is one significant intramolecular H···H contact of 2.29(7) Å between H(2) atom of ferrocenyl and H(13B) of adamantyl, which is by 0.11 Å shorter than the sum of the van der Waals radii. The mutual crowding imposed by the substituents is further reflected on bending of the link between C(11), C(1) and the centroid of the cyclopentadienyl (the corresponding angle is 175.1(4)°) in the direction which releases the crowding at least partially; a similar effect originates from tilting of the mean plane of the ketonic unit relatively to cyclopentadienyl, as demonstrated by the torsion angles –169.4(4)° and 7.6(3)° for C(2)–C(1)–C(11)–O and C(5)–C(1)–C(11)–O, respectively.

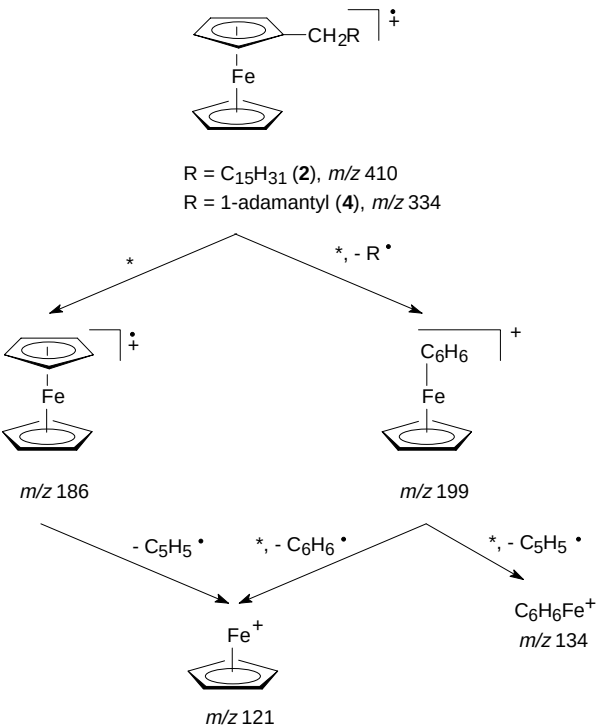

SCHEME 3

In contrast, the adamantyl substituent, apart from some opening of the angles C(11)–C(12)-cage carbons, remains essentially undistorted: the mean C–C distance and C–C–C angle within the cage is 1.530(11) Å and 109.6(9)°, respectively.

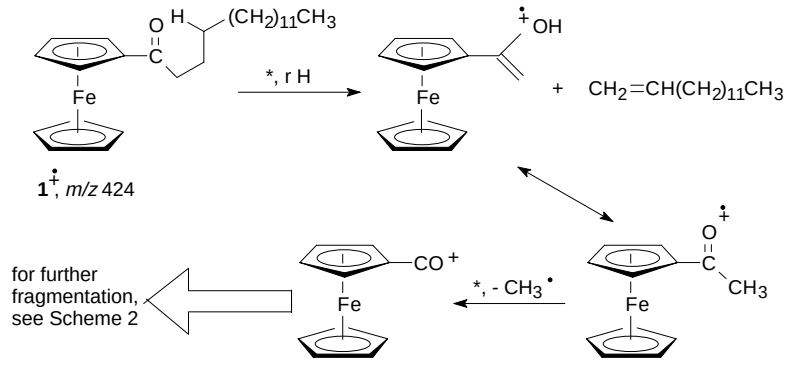

SCHEME 4

Ferrocene derivatives were studied in detail by ^{57}Fe Mössbauer spectroscopy, in some cases in connection to theoretical calculations. Due to small changes of the 4s-electron density at the central iron atom (isomer shift IS = $\alpha_{Fe}(|\psi_{sample}(0)|^2 - |\psi_{source}(0)|^2)$, where $|\psi(0)|^2$ is the electron density at the nucleus and α_{Fe} the proportionality constant; negative in the case of ^{57}Fe), the IS values for non-bridged ferrocenes are relatively independent of the nature of the ring substituents[10]. The changes of electron density distribution at iron nucleus are more significantly reflected on the quadrupole splitting (QS) values. Due to the positive sign of the electric field gradient at the iron nucleus,

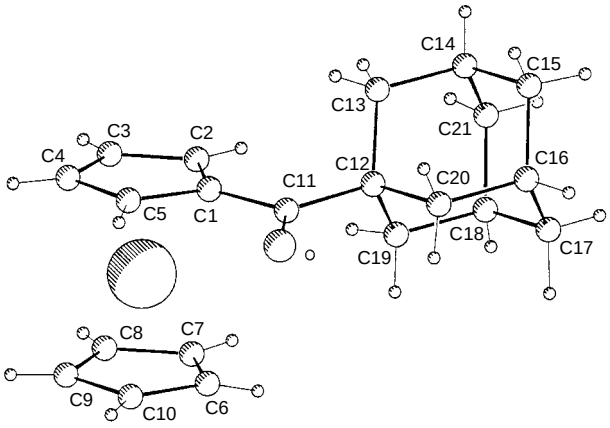

FIG. 1
Perspective view of **3** with atom labelling

TABLE III
Selected bond lengths (Å) and angles (°) for compound **3**

Atoms	Bond lengths	Atoms	Angles
Fe–C(Cp) mean	2.030(5)	C–C–C(Cp) mean	108.0(6)
C1–C2	1.453(6)	O–C11–C1	118.4(4)
C1–C5	1.416(7)	O–C11–C12	119.7(4)
C2–C3	1.399(7)	C2–C1–C11	131.2(5)
C3–C4	1.396(7)	C5–C1–C11	121.7(4)
C4–C5	1.408(7)	C1–C11–C12	121.8(4)
C6–C7	1.395(9)	C11–C12–C13	111.7(4)
C6–C10	1.387(9)	C11–C12–C19	110.5(3)
C7–C8	1.396(9)	C11–C12–C20	109.2(4)
C8–C9	1.388(9)	C13–C12–C19	109.6(4)
C9–C10	1.411(9)	C13–C12–C20	107.8(4)
C11–O	1.220(5)	C19–C12–C20	107.8(4)
C1–C11	1.488(6)	C14–C13–C12	110.2(4)
C11–C12	1.530(6)	C13–C14–C15	110.0(4)
C12–C13	1.528(6)	C13–C14–C21	109.4(4)
C12–C19	1.541(6)	C15–C14–C21	109.7(5)
C12–C20	1.546(6)	C16–C15–C14	109.3(4)
C13–C14	1.524(7)	C15–C16–C20	109.8(4)
C14–C15	1.525(7)	C15–C16–C17	109.6(4)
C14–C21	1.538(8)	C20–C16–C17	108.9(5)
C15–C16	1.512(7)	C18–C17–C16	109.7(4)
C16–C20	1.524(7)	C17–C18–C21	110.1(5)
C16–C17	1.531(7)	C17–C18–C19	109.6(5)
C17–C18	1.520(7)	C21–C18–C19	108.3(4)
C18–C21	1.523(8)	C12–C19–C18	109.9(3)
C18–C19	1.548(7)	C16–C20–C12	111.0(4)
		C18–C21–C14	109.4(4)

the higher value of QS indicates the increase of population of the d_{xy} and d_{x2-y2} orbitals and/or the decrease of population of the d_{xz} and d_{yz} orbitals (assuming the population of the non-bonding d_{z2} orbital being constant)[11]. The examples are as follows [compound, IS (mm s^{-1}), QS (mm s^{-1})]: 80 and 77 K: FcH 0.53, 2.37; FcAc 0.53, 2.24; FcCOOH 0.53, 2.21 (ref.[11]) and $FcCH_3$ 0.53, 2.39 (ref.[12]) (Fc = (η^5-C_5H_5)Fe(η^5-C_5H_4)); room temperature: FcH 0.44, 2.42 (ref.[13]). The data of the compounds **1–4** and for ferrocene (measured for comparison) are given in Table IV.

Due to the temperature dependence of ^{57}Fe IS values (0.02–0.1 mm s^{-1}/100 K; ref.[10]), only the trends in IS and QS are comparable with the previously cited data. The values of IS and QS for FcH are in a fairly good agreement with literature data (see above). As expected, the IS values for **1–4** are mutually very close. On the other hand, the QS values reflect the electronic properties of the substituents: FcH ≈ **2** > **4** >> **1** > **3**.

TABLE IV
Isomer shift, quadrupole splitting and D_{21} values for ferrocene and compounds **1–4**

Parameter	FcH	**1**	**2**	**3**	**4**
IS, mm s^{-1}	0.447	0.435	0.443	0.431	0.439
QS, mm s^{-1}	2.389	2.274	2.383	2.229	2.325
D_{21}[a]	1.106	0.805	0.682	1.191	1.190

[a] D_{21} is defined as the ratio of the areas of the doublet components originating from m_I: ±3/2 ←±1/2 and ±1/2 ←±1/2 transitions; m_I is the magnetic quantum number.

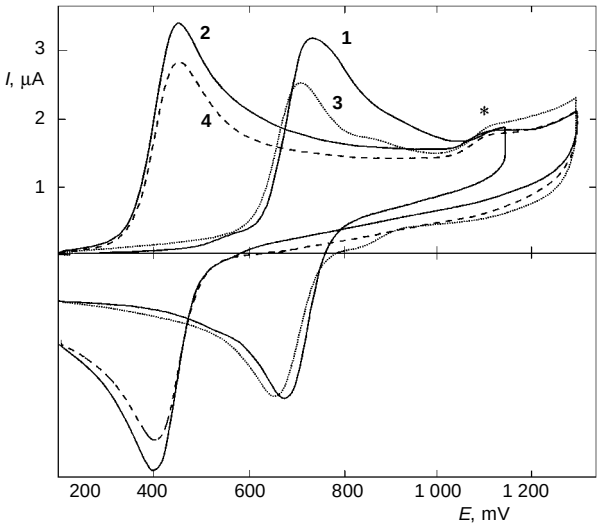

FIG. 2
Cyclovoltammograms of **1–4**. See Experimental for details. The asterisk denotes wave of supporting electrolyte

This is in accord with the general observation[14] that the presence of electron-withdrawing substituents lead to changes of electron density within ferrocene moiety and, simultaneously, to the decrease of electron distribution anisotropy on orbital energy lowering.

As the recoilless fraction of the γ-absorption is anisotropic[15], the observed asymmetry of the quadrupole doublets in Mössbauer spectra of diamagnetic compounds can be either the result of preferential orientation of the samples or the consequence of the Goldanskii–Karyagin effect. Considering the nature of the samples which are more or less waxy solids, the asymmetry in the intensities looks to be caused by anisotropy of orientation of the samples during the mounting. This is supported by the fact that the greatest difference of D_{21} from unity appears for derivatives with the long aliphatic chain (**1**, **2**), the solid samples of which are composed of waxy-like flakes.

The electrochemical behavior of **1–4** does not differ significantly. Only one main anodic process (Table V, Fig. 2) observed represents an one-electron oxidation of the ferrocene skeleton to give the corresponding ferricinium. This process is reversible in the range of the polarization rates applied (10–200 mV s^{-1}) and independent of the electrode material (Au or GC). The trend of the $E_{1/2}$ values **1** > **3** > FcH > **2** ≥ **4** reflects the decrease of the electron density within the ferrocene skeleton and, simultaneously, the lowering of the ferrocene orbital energies on substitution with an electron-withdrawing group (see above). This makes the ferrocene moiety more resistant towards oxidation to the ferricinium ions. This trend is the same as that of the electron donating ability of the substituents (1-adamantylmethyl) > hexadecyl > H > (1-adamantanecarbonyl) > palmitoyl as illustrated by the Hammett's σ_p constants: $\sigma_p(CH_3CO)$ 0.50 > σ_p(H) 0 > $\sigma_p(CH_3)$ –0.17 > $\sigma_p((CH_3)_3C)$ –0.20. The electron-accepting

TABLE V
Electrochemical data[a] for compounds **1–4**

Compound	Electrode	E_{pa}, mV	I_{pa}, μA	$E_{1/2}$, mV	$D \cdot 10^{10}$, m^2 s^{-1}
FcH	Au	510	7.3	480	6.99
1	Au	745	8.35	715	1.53
	GC	745	3.09	715	1.24
2	Au	450	9.25	420	1.88
	GC	455	3.38	425	1.48
3	Au	710	8.2	680	1.47
	GC	710	2.5	680	0.83
4	Au	460	7.7	430	1.3
	GC	455	2.9	425	1.1

[a] E_{pa} (I_{pa}) potential (current) of the anodic wave in CV, $E_{1/2}$ half-wave potential, D diffusion coefficient.

ability of (1-AdaCO) group is lower than that of palmitoyl group as a result of the presence of three β C–C bonds, through which the electron deficiency is compensated. This difference is, however, smaller for the pair (1-AdaCH_2)/hexadecyl.

In the case of **3** at Au-electrode, additional weak I_{pa}/I_{pa}(main) ratio 0.065) one-electron reversible wave was observed, which is shifted to higher potential ($E_{1/2}$ 880 mV). This process is faradaic in nature on the basis of AC voltammetry (adsorption or capacitance processes are excluded) but its origin remains obscure. On the other hand, the main component of cyclic voltammogram of **3** exhibits considerable changes during repeated CV-runs on both Au and GC electrodes (decrease of I_{pa}, increase of ΔE_p; Fig. 3) indicating the adsorption on the electrode surface. Possible causes of this phenomena are, among others, the adsorption of the parent ferrocene derivative and/or the adsorption of the corresponding ferricinium.

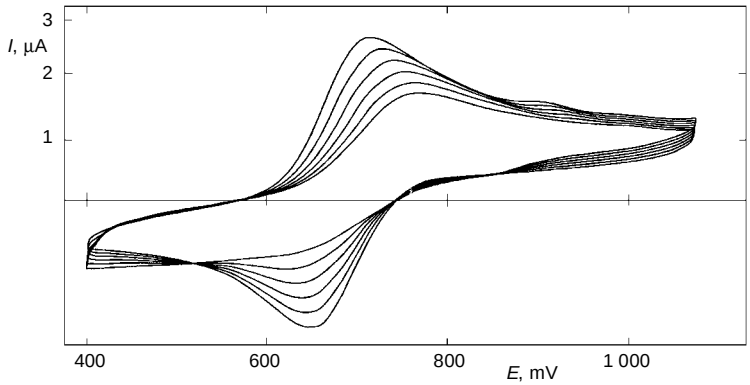

FIG. 3
Changes in cyclovoltammogram of **3** on repeated scanning. The highest amplitude corresponds to the first scan

The small differences in the diffusion coefficient values of **1–4** indicates that the sizes of the ferricinium ions are similar under the given conditions (nitrobenzene as the solvent). The results demonstrate that the introduction of proper substituents on the ferrocene skeleton makes it possible not only to tune the redox potential (which remains stable and reversible) but also more subtle effects such as solubility, diffusion coefficients and surface tension may be controlled.

REFERENCES

1. Gubin S. P., Smirnova S. A., Denisovich L. I., Lubovich A. A.: J. Organomet. Chem. *30*, 243 (1971).
2. Hillman A. R., Taylor D. A., Hamnett A., Higgins S. J.: J. Electroanal. Chem. *266*, 423 (1989); and references therein.

3. Little W. F., Reilley C. N., Johnson J. D., Sanders A. P.: J. Am. Chem. Soc. *86*, 1382 (1964); Perevalova E. G., Gubin S. P., Smirnova S. A., Nesmeyanov A. N.: Dokl. Akad. Nauk SSSR *155*, 857 (1964); and references therein.
4. Slocum D. W., Ernst C. R. in: *Advances in Organometallic Chemistry* (F. G. A. Stone and R. West, Eds). Academic Press, New York 1972.
5. Nicholson R. S., Shain I.: Anal. Chem. *36*, 706 91964).
6. Vogel M., Rausch M., Rosenberg H.: J. Org. Chem. *22*, 1016 (1957).
7. Altomare A., Burla M. C., Camalli M., Cascarano G., Giacovazzo C., Guagliardi A., Polidori G.: J. Appl. Cryst. *27*, 435 (1994).
8. Sheldrick G. M.: *SHELXL93. Program for Crystal Structure Refinement from Diffraction Data*. University of Göttingen, Göttingen 1993.
9. Mandelbaum A., Cais M.: Tetrahedron Lett. *51*, 3847 (1964).
10. Vertes A., Korecz L., Burger K.: *Mössbauer Spectroscopy*, pp. 13–52 and 123–186. Akadémiai Kiado, Budapest 1979.
11. Korecz L., Abou H., Ortaggi G., Graziani M., Belluco U., Burger K.: Inorg. Chim. Acta *9*, 209 (1974).
12. Nagy A. G., Deszi I., Hillman M.: J. Organomet. Chem. *117*, 55 (1976).
13. Osborne A. G., Whiteley R. H., Meads R. E.: J. Organomet. Chem. *193*, 345 (1980).
14. Sosinsky B. A. in: *Chemical Mössbauer Spectroscopy* (H. B. Herber, Ed.), p. 1–25. Plenum Press, New York 1974.
15. Gibb T. C.: *Principles of Mössbauer Spectroscopy*, pp. 38–43 and 143–156. Chapman and Hall, London 1976.